Hindawi
Journal of Nanomaterials
Volume 2017, Article ID 3475248, 12 pages
https://doi.org/10.1155/2017/3475248

Research Article

Preparation of a Leaf-Like $BiVO_4$-Reduced Graphene Oxide Composite and Its Photocatalytic Activity

Shimin Xiong,[1,2] Tianhui Wu,[1] Zihong Fan,[3] Deqiang Zhao,[1] Mao Du,[1] and Xuan Xu[1,4]

[1] *Key Laboratory of Three Gorges Reservoir Region's Eco-Environment, Ministry of Education, Chongqing University, No. 174 Shazhengjie, Shapingba, Chongqing 400045, China*
[2] *Luzhou Laojiao Company Limited, No. 9 Nanguang Road, Longmatan District, Luzhou City, Sichuan Province 646006, China*
[3] *Chongqing Key Laboratory of Catalysis and Functional Organic Molecules, College of Environment and Resources, Chongqing Technology and Business University, Chongqing 400067, China*
[4] *National Center for International Research of Low-Carbon and Green Buildings, Chongqing University, Chongqing 40004, China*

Correspondence should be addressed to Xuan Xu; xuxuan@cqu.edu.cn

Received 25 October 2016; Revised 1 January 2017; Accepted 26 February 2017; Published 3 April 2017

Academic Editor: Qin Hu

We prepared a unique leaf-like $BiVO_4$-reduced graphene oxide ($BiVO_4$-rGO) composite with prominent adsorption performance and photocatalytic ability by a single-step method. Multiple characterization results showed that the leaf-like $BiVO_4$ with average diameter of about 5 um was well dispersed on the reduced graphene oxide sheet, which enhanced the transportation of photogenerated electrons into $BiVO_4$, thereby leading to efficient separation of photogenerated carriers in the coupled graphene-nanocomposite system. The characterization and experiment results also indicated that the outstanding adsorption ability of such composite was closely associated with the rough surface of the leaf-like $BiVO_4$ and doped rGO. The surface photocurrent spectroscopy and transient photocurrent density measurement results demonstrated that the doped rGO enhanced separation efficiency and transfer rate of photogenerated charges. As a result, the $BiVO_4$-rGO exhibited higher photocatalytic capacity toward the degradation of rhodamine B dye under visible-light irradiation compared with pure $BiVO_4$ and P25.

1. Introduction

In the world where energy shortage and environment pollution have become worse, semiconductor-based photocatalysis has attracted great attention over the past decades because of its potential applications in solar energy conversion and environmental purification [1–3]. To prepare high-activity photocatalysts, researchers have made numerous attempts to prepare new ones such as TiO_2, $(BiO)_2CO_3$, ZnO, and $BiVO_4$ [4–7]. Considering that visible light accounts for the largest proportion of the solar spectrum and artificial light, preparation of a high-activity visible-light-driven photocatalyst has become a hot topic at present [8].

As a visible-light-driven photocatalyst, $BiVO_4$ enjoys advantageous properties such as nontoxicity, low cost, and high stability against photocorrosion. The bandgap of monoclinic $BiVO_4$ is 2.4 eV, which means it can be successfully activated by visible light. Recently, more and more attention has been paid to the synthesis of $BiVO_4$ of different sizes and shapes. Since the morphology of $BiVO_4$ will significantly impact its photocatalytic performance, researchers have synthesized $BiVO_4$ in various morphological shapes such as $BiVO_4$ nanosheets [9, 10], peanut-like $BiVO_4$ [11], spherical $BiVO_4$ [12], flower-like $BiVO_4$ [13], three-dimensional acicular sheaf $BiVO_4$ [14], and tube-like $BiVO_4$ [8], so as to better tune the photocatalytic capacities of materials and thus realize enhanced degradation of pollutants. However, pure $BiVO_4$ has limited efficiency in migration of photogenerated electron-hole pairs, which restricts its application in practical situations [15]. To solve this problem, great efforts have been conducted, for instance, incorporating reduced graphene oxide into the monoclinic $BiVO_4$ [16, 17].

It is a reliable way to improve the photocatalytic activity of pure $BiVO_4$ by coupling with graphene-related materials (e.g., reduced graphene oxide (rGO)). With two-dimensional conjugated structure and unique intrinsic

properties, graphene (as well as rGO) can serve as a supporting platform on which semiconductors can be dispersed and stabilized for being applied in catalysis [18]. rGO enjoys high electrical conductivity, high carrier mobility (200000 cm^2/V), high specific surface area (2630 m^2/g), and a bandgap which is almost zero [19–21]. Therefore, it is a preferred material for loading catalysts, transporting electrons, and stabilizing extraneous electrons. It is worth noting that graphene has outstanding electronic conductivity because of its high abundance of delocalized electrons in its π-conjugated electronic structure. In the graphene-composite coupled system, the high conductivity of graphene facilitates an effective transfer of photogenerated charges in the attached semiconductors, thus leading to efficient separation of photogenerated charge carriers [12, 22, 23].

There have been few comparative researches on lamellar $BiVO_4$-graphene nanocomposite and microspherical silver-rGO-$BiVO_4$ composite [12, 22]. These researches revealed that the morphology of the catalyst has great influence on its photocatalytic activity. In this study, a single-step method was adopted to synthesize a leaf-like $BiVO_4$-rGO composite, of which the photocatalytic activity was tested via degradation of rhodamine B.

2. Experiments

2.1. Materials. In this experiment, we used analytically pure chemicals including bismuth(III) nitrate pentahydrate ($Bi(NO_3)_3{\cdot}5H_2O$, Chengdu Kelong Chemical Company), ammonium metavanadate (NH_4VO_3, Chongqing Chuandong Chemical Company), sodium hydroxide (NaOH, Chongqing Chuandong Chemical Company), nitric acid (HNO_3, Chengdu Kelong Chemical Company), rhodamine B (RhB) dye (Tianjin Guangfu Fine Chemical Research Institute), and graphene oxide water solution (GO solution, ≥99.85%, with concentration of 2 mg/mL, Hengqiu Tech Company).

2.2. Synthesis of $BiVO_4$-rGO Composite. Dissolve 0.01 mol $Bi(NO_3)_3{\cdot}5H_2O$ in 50 mL of 2 mol/L HNO_3 solution, and then mark the solution as solution A. In contrast, dissolve 0.01 mol NH_4VO_3 in 50 mL of 2 mol/L NaOH solution, and then mark the solution as solution B. After that, add solution B dropwise to solution A while stirring for 30 min. Adjust the pH of the mixed solution to 7 by adding 2 mol/L NaOH solution dropwise. In addition, add 8.2 mL of 2.0 mg/mL GO solution to 20 mL of DI water, and then conduct sonication treatment in an ultrasonic bath for about 1 h. Subsequently, add GO solution to the $BiVO_4$ mixed solution followed by sonication treatment for another 1 h. After the above procedures, a homogeneous suspension is formed, and thus the sample can be obtained. Place the sample in a 100 mL Teflon-sealed autoclave at 200°C for 6 h before realizing the crystallization of $BiVO_4$ and GO composite and the reduction of GO. Conduct centrifugation treatment for the precipitate, wash it with deionized water several times, and then dry it in the vacuum freeze drier at −60°C for 24 h, finally obtaining the synthesized composite known as $BiVO_4$-rGO (wherein the mass percentage of rGO is 0.5%). For comparison, implement the same procedures to synthesize pure $BiVO_4$.

2.3. Characterization. Scanning electron microscopy (SEM) images were obtained using a JSM-7800F JEOL emission scanning electron microscope; energy dispersive X-ray (EDX) images were obtained using an EDX-100A-4; powder X-ray diffraction (XRD) spectra were obtained using a Rigaku D/Max-rB diffractometer with Cu Kα radiation. The scanning angle 2θ ranged between 10° and 70°. UV-visible diffuse-reflectance spectroscopy (UV-Vis DRS) was performed using Hitachi U-3010 UV-Vis spectrometer. Fourier transform infrared spectroscopy (FTIR, IRPrestige-21, Shimadzu, Japan) analysis of the composite was conducted using FTIR spectrophotometer by using KBr as a reference sample. An Al Ka X-ray source (Thermo Fischer Scientific, K-Alpha, UA) was adopted to conduct X-ray photoelectron spectroscopy (XPS) characterization. Photoelectrochemical properties were evaluated using a CHI Electrochemical Workstation (CHI 760E, Shanghai Chenhua, China). The sample for electron spin resonance (ESR) measurement was prepared by mixing photocatalyst powder samples in a 50 mM DMPO solution tank (aqueous dispersion for DMPO-$^{\bullet}OH$ and methanol dispersion for DMPO-$O_2^{\bullet-}$). The Brunauer-Emmett-Teller (BET) surface area measurements and evaluation of the porosities of the samples were conducted on the basis of nitrogen adsorption isotherms measured at 400°C using a gas adsorption apparatus (Gemini VII 2390, Micromeritics Instrument Corp., Norcross, GA, USA).

2.4. Evaluation of Photocatalytic Activity. The photocatalytic activities of the samples were evaluated via photodegradation of RhB using a 500 W Xe lamp as visible-light irradiation source at room temperature. In this experiment, first add 0.10 g catalyst to 100 mL of a 5 mg/L RhB aqueous solution, and then keep magnetically stirring for 30 min in the dark to obtain good dispersion and reach adsorption-desorption equilibrium between the dye and the catalyst. After that, place the solution in a 250 mL beaker, which is located 350 mm away from the 500 W Xe lamp. Collect the solution once for every 2 h of irradiation, and then subject it to centrifugation at 10000 r/min for removing catalysts, and finally test the absorbance of RhB in the solution. The concentration of the remaining dye was spectrophotometrically monitored according to the absorbance of the solutions at 552 nm. For comparison, the control experiments were performed with pure $BiVO_4$, P25, and $BiVO_4$-rGO (with different mass percentages of rGO), or without any catalyst under the same condition. To investigate the effect of rGO dosage on the photocatalytic property of the photocatalyst, the $BiVO_4$-rGOs with rGO wt% of 0.25, 0.5, and 1 were synthesized, respectively.

3. Results and Discussion

3.1. SEM-Based Morphology Analysis. Scanning electron microscopy (SEM) was used to study the sizes and morphologies of the prepared samples. As shown in

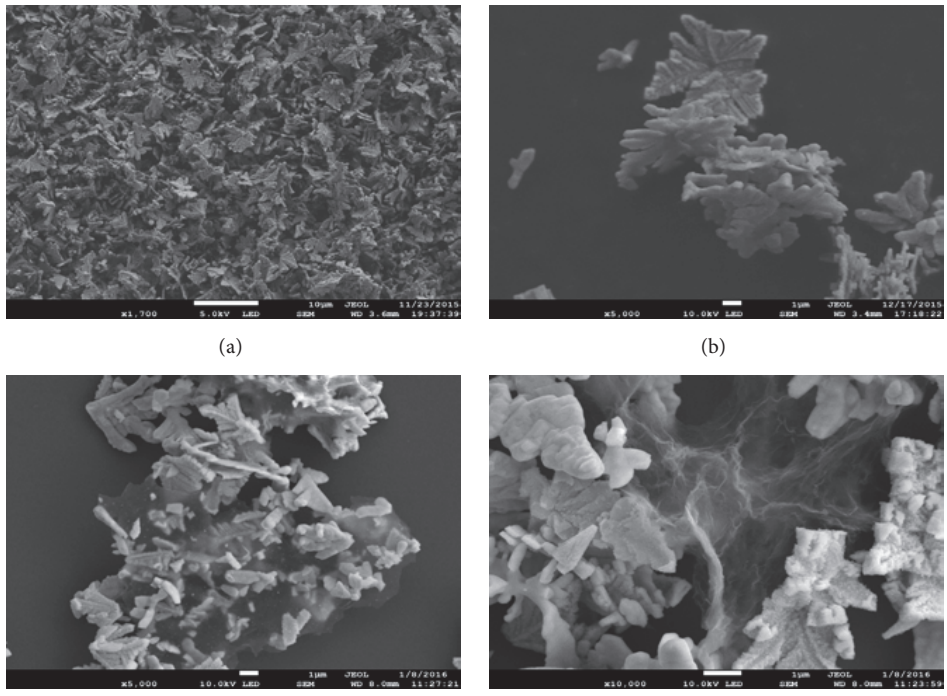

(a) (b)

(c) (d)

Figure 1: SEM images of ((a), (b)) pure $BiVO_4$ and ((c), (d)) $BiVO_4$-rGO.

Figure 1, each sample has a unique leaf-like structure consisting of $BiVO_4$ crystal grains of which the average diameter is about 5 um, and the rGO sheet within is easy to be observed. According to Figures 1(c) and 1(d), it can be seen that the two leaf-like $BiVO_4$ structures are loaded on the rGO sheets. Since $BiVO_4$ and rGO sheets are closely in contact with each other, transportation of electrons photogenerated in $BiVO_4$ can be enhanced, thereby leading to efficient separation of photogenerated carriers in the coupled rGO-composite system. In conclusion, this material is expected to have enhanced photocatalytic activity.

3.2. EDX-Based Composition Analysis. The chemical composition of $BiVO_4$-rGO was measured by studying its EDX spectrum. Figure 2 shows that $BiVO_4$-rGO is mainly composed of elements Bi, C, O, and V. Based on the elemental mapping images, we can draw the following conclusion. First, the leaf-like particles are bismuth vanadate, because their distributions of Bi, O, and V are almost the same; second, the surface of $BiVO_4$ is covered with a layer of rGO film, because the color of C element is determined by rGO film's positon. According to the SEM and EDX results, it can be known that the leaf-like $BiVO_4$ particles are successfully loaded on the surface of the rGO film, which is consistent with XRD results.

3.3. XRD Pattern Analysis. The phase structures of the composites were characterized by X-ray diffraction (XRD) measurement and the XRD patterns are shown in Figure 3. The sharp XRD peaks indicate that the $BiVO_4$ is in high crystallinity. From this figure, we can see that almost all the diffraction peaks (110, 010, 121, 040, 200, 211, 150, 240, 161, etc.) of the pure $BiVO_4$ and $BiVO_4$-rGO could be ascribed to the monoclinic $BiVO_4$ (JCPDS 14-0688) [24] which is the most active phase of three phases of $BiVO_4$ under visible-light irradiation [25]. This explains why the photocatalysts remain in a monoclinic structure and why the phase of $BiVO_4$ remains unchanged after the addition of GO. An insignificant peak (002, with blue color) of rGO at around 25° can be observed while no characteristic peak of GO at around 12° can be found, which indicates that GO has been well reduced to rGO through the photocatalytic reduction process [18, 26]. The XRD analysis also shows that the phase of $BiVO_4$ remains unchanged after the addition of GO.

3.4. Analysis of Optical Properties Based on UV-Vis DRS. The optical absorption property of the semiconductor has been regarded as a key influencing factor on its photocatalytic performance. Figure 4 shows representative spectra of pure $BiVO_4$ and $BiVO_4$-rGO, respectively, from which we can see that the absorption spectrum of $BiVO_4$-rGO is nearly the same as that of pure $BiVO_4$, and the spectrum of $BiVO_4$-rGO is above that of pure $BiVO_4$. These results verify that the incorporation of rGO can lead to significantly increased absorption of visible light, therefore increasing the utilization of visible light.

Moreover, the energy band structure of semiconductor is also an important factor determining its photocatalytic

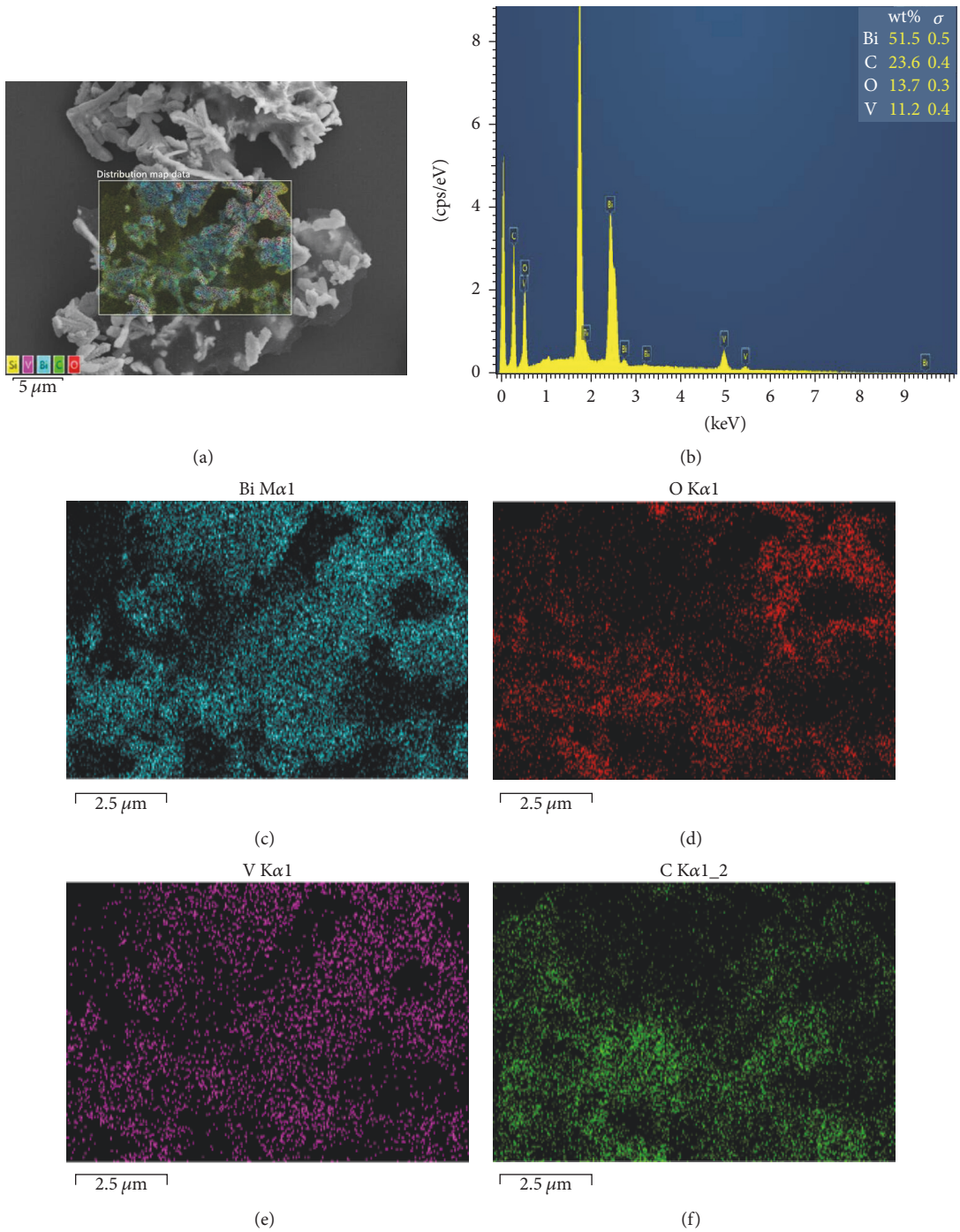

FIGURE 2: (a) SEM image of composite $BiVO_4$-rGO; (b) EDX spectrum of composite $BiVO_4$-rGO; ((c)–(f)) SEM elemental distribution mappings of Bi, O, V, and C.

activity. The relationship of absorbance and incident photon energy hv can be described by

$$Ahv = C\left(hv - E_g\right)^{1/2}. \quad (1)$$

In this equation, A represents the absorption coefficient, E_g represents the bandgap energy, h represents Planck's constant, v represents the incident light frequency, and C denotes a constant. The bandgap energy (E_g) of the photocatalyst can be estimated by a plot depicting $(Ahv)^2$ versus hv [27, 28]. The estimated bandgap energies of pure $BiVO_4$ and $BiVO_4$-rGO were measured to be 2.375 eV and 2.29 eV, respectively. The absorption edges of $BiVO_4$-rGO and pure $BiVO_4$ were measured to be 541.48 nm and 522.1 nm, respectively.

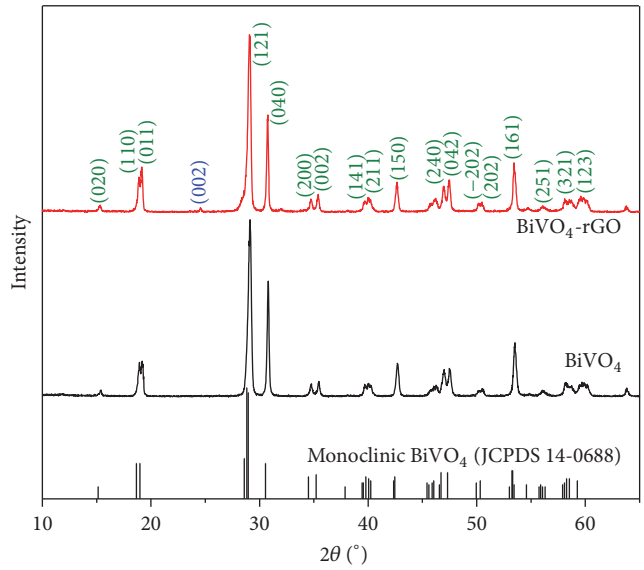

Figure 3: XRD patterns of pure $BiVO_4$, $BiVO_4$-rGO, and monoclinic $BiVO_4$ (JCPDS 14-0688).

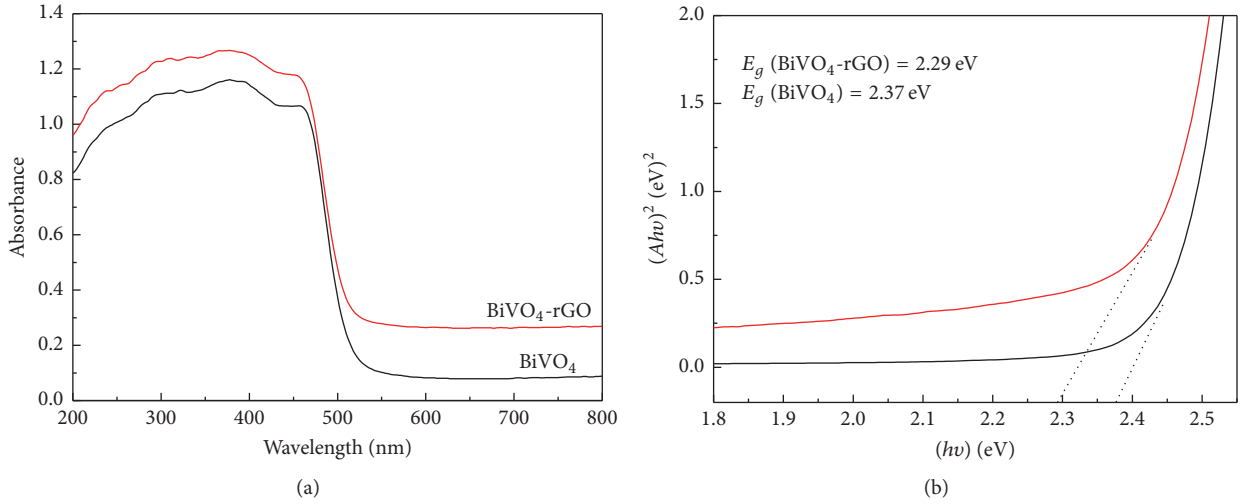

Figure 4: (a) UV-Vis DRS spectra. (b) The relationship between $(Ah\upsilon)^2$ and the photon energy ($h\upsilon$) of the as-synthesized pure $BiVO_4$ and $BiVO_4$-rGO.

3.5. FTIR-Based Chemical States Analysis. In order to ensure an efficient transfer of rGO and to characterize the carbon species, FIIR was used to obtain further insights into the reduction of GO. Figure 5 shows the FTIR spectra of GO, GR, $BiVO_4$, and $BiVO_4$-rGO, respectively. We can observe a strong absorption band of GO at 3410 cm^{-1} due to the O-H stretching vibration. The characteristic peaks at 1736, 1628, 1406, and 1089 cm^{-1} can be ascribed to carboxyl or carbonyl C=O stretching, carboxyl-OH stretching, C=C stretching, phenolic C-OH stretching, and alkoxy C-O stretching, respectively [29, 30]. In contrast to GO, the various oxygen-containing groups (800–1900 cm^{-1}) in $BiVO_4$-rGO and GR are significantly decreased or even disappeared, indicating that the hydrothermal synthesis is an effective method for reducing GO into rGO. In the case of the $BiVO_4$-rGO, the typical absorption peaks of GO are dramatically weakened or even disappeared as compared with those of the pure GO, which verifies the reduction action of GO. The broad absorption cases at low frequency (below 1000 cm^{-1}) are associated with ν_1 (VO_4) and ν_3 (VO_4) [31]. All the results show that, in our study work, we can successfully prepare a composite catalyst which incorporates rGO as a platform.

3.6. XPS-Based Chemical States Analysis. XPS was used to evaluate the chemical and bonding environments of loaded $BiVO_4$-rGO, and results are shown in Figure 6. As shown in Figure 6(a), the scanned spectrum of $BiVO_4$-rGO is within the range between 0 and 800 eV, from which we can find that this composite consists of elements Bi, O, V, and C. Figure 6(b) shows the binding energies for Bi $4f_{7/2}$ and Bi

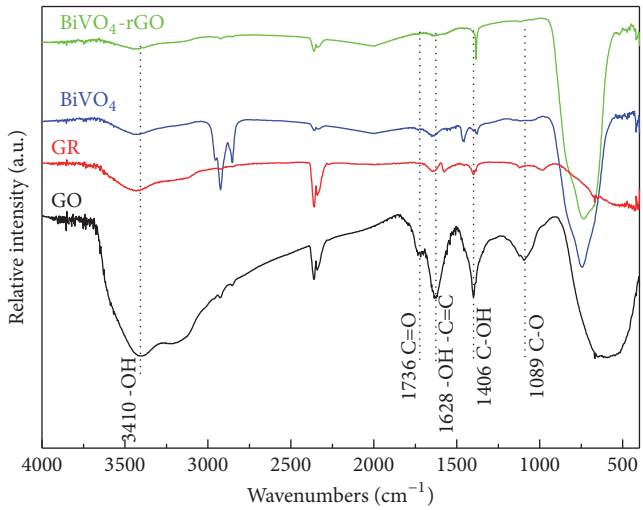

Figure 5: FTIR spectra of GO, GR, pure $BiVO_4$, and $BiVO_4$-rGO.

$4f_{5/2}$ to be 158.8 and 164.1 eV, respectively, which is closely associated with the Bi^{3+} peak in the monoclinic $BiVO_4$ [32]. Figure 6(c) shows the C1s XPS spectrum, in which we can see two characteristic peaks that are caused by the oxygenated ring C bonds (284.6 eV for C-C, C=C, and C-H and 287.0 eV for the C-O bond) [33]. These results indicate that some oxygen-containing functional groups are loaded on the rGO surface. Due to the presence of these groups, pollutants can be absorbed by catalysts more easily, and the photocatalytic effect of the catalyst can be enhanced. However, in the C1s XPS spectra of $BiVO_4$-rGO, the relative intensities of the three components associated with C-O/C-O bonds decrease significantly, which indicates that some of the oxygen functional groups were reduced during the reduction process [34]. Although the GO makes no contribution to the transfer of electron because of nonconductivity, the GO after reduction (rGO) is significantly helpful. According to Figure 6(e), it can be seen that the peaks at binding energies of 524.1 ($V2p_{1/2}$) and 516.3 eV ($V2p_{3/2}$) belong to the split signal of V2p, and the V2p peak is ascribed to V^{5+} [31].

3.7. Charge Separation Based on SPS and TPD. The photocatalytic ability of composite is also largely dependent on its capability of separating and transferring charges [35, 36]. The steady-state surface photocurrent spectroscopy is an effective approach to reveal the charge transfer efficiency of a semiconductor. In order to investigate the impact of rGO on the charge separation of $BiVO_4$, SPS was conducted in air atmosphere, and the SPS results are shown in Figure 7(a), from which we can observe strong signals for both samples. The deposited rGO on $BiVO_4$ could enhance the SPS response. Moreover, a stronger SPS response can lead to a higher charge separation rate [37]; therefore, it can be concluded that rGO can lead to enhanced charge separation of $BiVO_4$.

Photoelectrochemical measurements were conducted to study the excitation, separation, transfer, and recombination of photogenerated charge carriers [38]. As shown in Figure 7(b), $BiVO_4$-rGO electrode displays a prompt, steady, and reproducible photocurrent response during repeatedly switching on/off Vis irradiation, and lower photocurrent density is observed in the case of $BiVO_4$. The enhanced photocurrent of the $BiVO_4$-rGO electrode is associated with high photogenerated charge separation efficiency and high charge transfer rate in the composite. The rGO serves as an acceptor and also a transporter for the electrons excited by visible-light energy and generated from $BiVO_4$, so as to inhibit the recombination of photogenerated electron-hole pairs effectively.

Table 1: The degradation efficiency after 8 h and adsorption efficiency after 30 min of different photocatalysts.

Sample	Adsorption efficiency	Degradation efficiency
P25	0.04%	13%
$BiVO_4$	14%	37%
$BiVO_4$-rGO 0.25%	17%	49%
$BiVO_4$-rGO 1%	21%	59%
$BiVO_4$-rGO 0.5%	29%	75%

3.8. Photocatalytic Activity for Degradation of RhB. Figure 8 shows the photodegradation rates of RhB under visible-light irradiation by using $BiVO_4$-rGO (with rGO wt% of 0.25%, 0.5%, and 1%), pure $BiVO_4$, and P25, respectively. For comparison, the results of degradation of RhB without involvement of catalysts are also shown. Prior to irradiation, the mixture of the dye and catalyst was stirred in the dark for 30 min to attain adsorption-desorption equilibrium. Moreover, the photostability test was also evaluated.

From Figure 8(a) and Table 1, we can see that the concentrations of RhB in the presence of photocatalysts gradually decrease with the extending of visible-light irradiation time, while the concentration of RhB without the involvement of catalysts decreases insignificantly. This result indicates that the degradation of the RhB solution is affected by photocatalytic reaction under visible-light irradiation. After 8 h of irradiation, only about 3% of RhB was degraded without catalyst, which is mainly due to the self-sensitization induced photodegradation of RhB. In contrast, there were about 13%, 37%, 49%, 59%, and 75% of RhB photocatalytically degraded with P25, pure $BiVO_4$, $BiVO_4$-rGO-0.25%, $BiVO_4$-rGO-1%, and $BiVO_4$-rGO-0.5%, respectively. After stirring in the dark for 30 min, the adsorption percentages of P25, pure $BiVO_4$, $BiVO_4$-rGO-0.25%, $BiVO_4$-rGO-1%, and $BiVO_4$-rGO-0.5% were 0.04%, 14%, 17%, 21%, and 29%, respectively, which indicates that the leaf-like $BiVO_4$ photocatalyst is of excellent adsorption performance.

As shown in Figure 8(a), the photocatalytic ability of pure $BiVO_4$ is much stronger than that of P25 under visible-light irradiation. This is because the light response range of $BiVO_4$ is larger than that of P25 and the rough surface of special leaf-like $BiVO_4$ (in Figure 1, SEM pictures) can increase the reaction interface. In addition, the degradation rate of RhB when using the $BiVO_4$-rGOs as a catalyst was

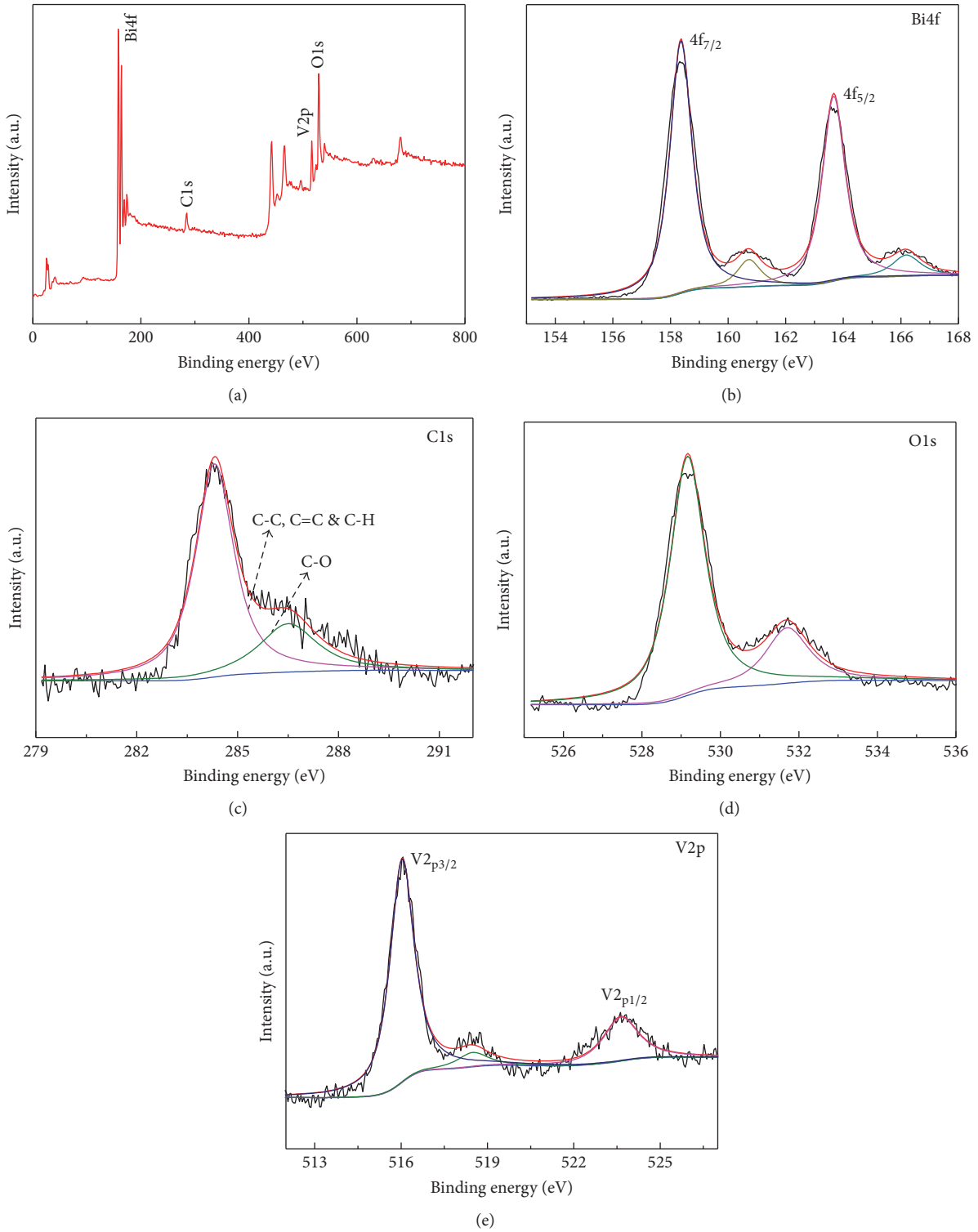

FIGURE 6: XPS spectra of the as-obtained $BiVO_4$-rGO. (a) Survey XPS spectrum; (b) Bi4f spectrum; (c) C1s spectrum; (d) O1s spectrum; (e) V2p spectrum.

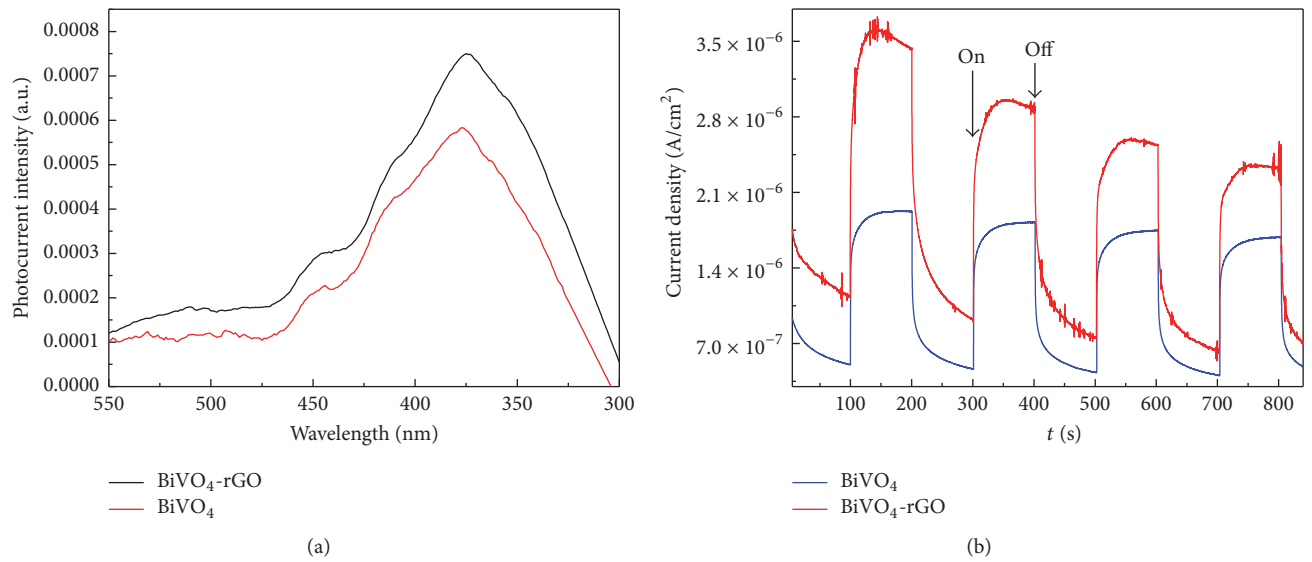

FIGURE 7: (a) The surface photocurrent spectroscopy (SPS) images of the as-obtained $BiVO_4$-rGO and pure $BiVO_4$. (b) The transient photocurrent densities (TPD) of the as-obtained $BiVO_4$-rGO and pure $BiVO_4$.

TABLE 2: Characteristics obtained from nitrogen desorption isotherms.

Sample	Mean pore size (nm)	Pore volume (cm^3g^{-1})	Surface area (m^2g^{-1})
$BiVO_4$	0.558	0.006381	2.199
$BiVO_4$-rGO 0.5%	3.5915	0.016921	8.0929

higher than that when using pure $BiVO_4$ as a catalyst. This is mainly due to the fact that $BiVO_4$-rGO has larger BET surface area and pore volume (Table 2), which further enhances the contact area between $BiVO_4$-rGO and organic contaminants. Moreover, the high electrical conductivity and high carrier mobility from rGO enhance the transfer of photogenerated electrons in the $BiVO_4$, thereby leading to efficient separation of photogenerated carriers in the coupled $BiVO_4$-rGO system and an increased photoconversion efficiency, which is consistent with the results of UV-Vis DRS, SPS, and TPD. We also studied the effect of the dosage of rGO on the photocatalytic properties of the photocatalyst, which can be ordered as $BiVO_4$-rGO-0.5% > $BiVO_4$-rGO-1% > $BiVO_4$-rGO-0.25%, indicating that the dosage of rGO indeed has a significant effect on both adsorption and degradation. The optimal dosage of rGO was finally determined as 0.5%. Although rGO can increase the surface area and facilitate the transfer of photogenerated electrons in the $BiVO_4$, an excessive dosage of rGO may lead to the shielding of the active sites of the photocatalysts, decreased contact area between $BiVO_4$ and light illumination, and lowered efficiency of light passing through the reaction solution, thereby reducing the photoactivity of $BiVO_4$-rGO composite [39].

Stability is another index greatly affecting the application of the catalyst. The stability of $BiVO_4$-rGO has been investigated, and the results are shown in Figure 8(c), from which we can see that there is no significant deactivation during the 4-cycle photodegradation process, and the slight decrease of photocatalytic activity is probably due to the mass loss during the centrifugation and washing process.

In order to investigate the photocatalytic mechanism, spin-trapping ESR technique was conducted to detect photogenerated radicals in the photocatalytic process, and results are shown in Figure 9. DMPO (5,5-dimethyl-1-pyrroline-N-oxide) is usually used for trapping radicals because of its capability of generating stable radicals such as the DMPO-hydroxyl radical ($^{\bullet}OH$) and DMPO-superoxide radical ($O_2^{\bullet-}$). The ESR technique was adopted to monitor the reactive species generated under the visible-light irradiation in the presence of $BiVO_4$-rGO and $BiVO_4$ in aqueous dispersion for DMPO-$^{\bullet}OH$ and in methanol dispersion for DMPO-$O_2^{\bullet-}$, and the results are shown in Figure 9. From the 4 pictures, we can clearly observe the signals of superoxide ($O_2^{\bullet-}$) and hydroxyl ($^{\bullet}OH$) radicals. The intensities of $O_2^{\bullet-}$ and $^{\bullet}OH$ signals of $BiVO_4$-rGO increase significantly after 9 min of irradiation, as shown in Figures 9(a) and 9(b). Therefore, $O_2^{\bullet-}$ and $^{\bullet}OH$ are the main oxidative species for the $BiVO_4$-rGO system which can react with RhB. As shown in Figure 9(c), the signal intensity of superoxide ($O_2^{\bullet-}$) of $BiVO_4$-rGO is stronger than that of $BiVO_4$, which can also be observed in Figure 9(d).

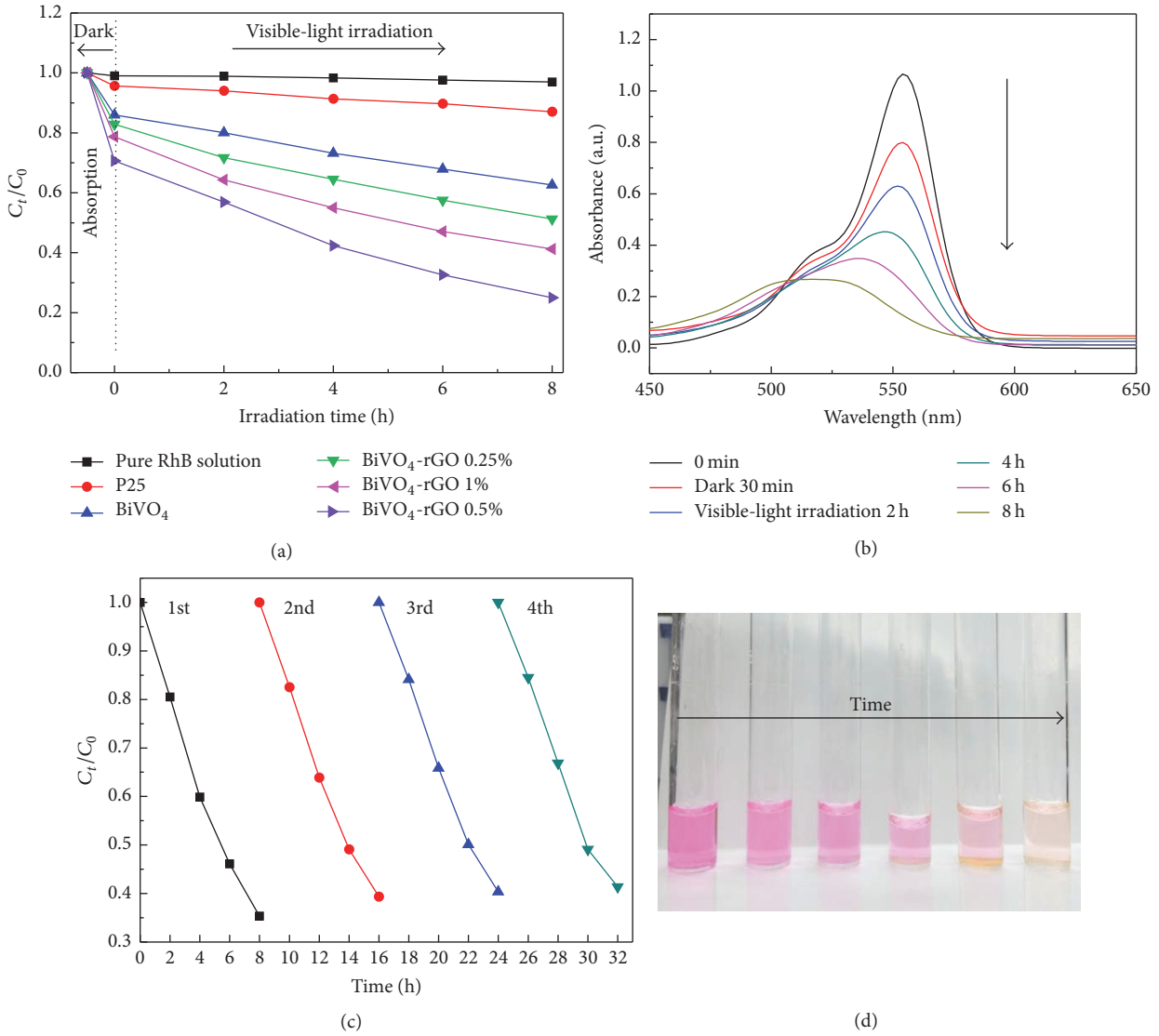

FIGURE 8: (a) The concentration ratio of the remaining RhB with different catalysts under visible-light irradiation. ((b), (d)) Photocatalytic performance of $BiVO_4$-rGO 0.5% for the decolorization of RhB as measured by UV-Vis DRS and pictures. (c) The photostability test of $BiVO_4$-rGO 0.5% for the cycling photodegradation of RhB under visible-light irradiation.

A possible reaction process is proposed in Figure 10. Electron-hole pairs are first generated on the $BiVO_4$ surface under visible-light excitation, and then photogenerated electrons are quickly transferred to rGO sheets via the percolation mechanism. After that, the electrons on rGO sheets react with O_2, resulting in $^{\bullet}O_2^-$ radicals and $^{\bullet}OH$. Finally, the dye molecules adsorbed on the active sites of $BiVO_4$-rGO are oxidized by the active species (h^+, $^{\bullet}OH$, and $O_2^{\bullet-}$). In the whole process, the rGO sheet serves as an electron mediator, which is of enhancing effect for the separation and transfer of electrons.

4. Conclusions

In summary, a simple and low-cost method was proposed for the controllable synthesis of leaf-like $BiVO_4$-rGO under gentle conditions. The as-synthesized composite $BiVO_4$-rGO exhibited excellent performances in adsorption and photocatalytic degradation of RhB in aqueous solution. After being incorporated with rGO, the leaf-like $BiVO_4$ displayed an enhanced photocatalytic activity, enhanced light harvesting efficiency, and reduced charge recombination rate due to its unique morphological structure. In addition, the as-prepared $BiVO_4$-rGO showed good photocatalytic repeatability and stability under irradiation for a prolonged time. This research, in which a unique shaped semiconductor was combined with rGO, provides reference for designing novel hybrid photocatalysts that may effectively solve water-pollution issues.

Conflicts of Interest

The authors declare that there are no conflicts of interest regarding the publication of this paper.

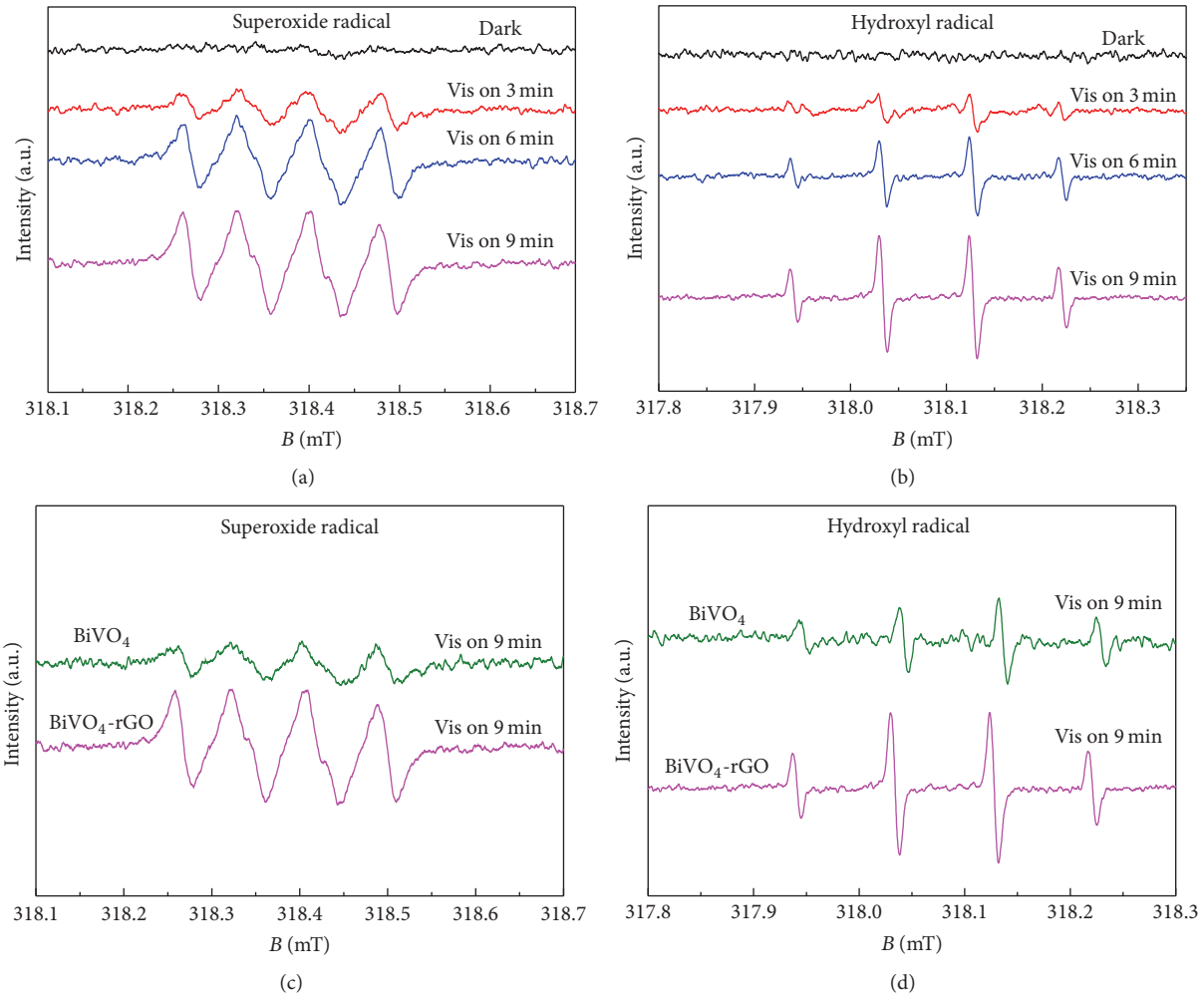

Figure 9: DMPO spin-trapping ESR spectra of $BiVO_4$-rGO during different times (a) in aqueous dispersion for $O_2^{\bullet-}$ and (b) in methanol dispersion for $^{\bullet}OH$; the DMPO spin-trapping ESR spectra of $BiVO_4$-rGO and $BiVO_4$ under Vis irradiation for 9 min (c) for $O_2^{\bullet-}$ and (d) for $^{\bullet}OH$.

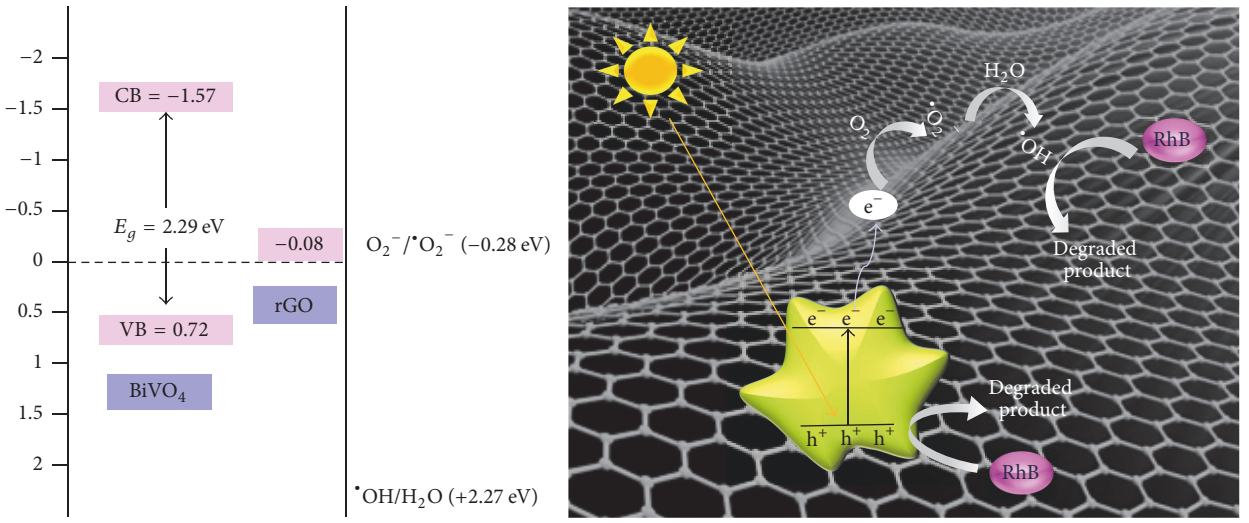

Figure 10: Photocatalytic reaction mechanism of $BiVO_4$-rGO.

Acknowledgments

Financial support from the Science and Technology Innovation Special Projects of Social Undertakings and Livelihood Support, Chongqing (cstc2015shmsztzx20003, cstc2016shmszx20009), the Science and Technology Project of Chongqing Education Commission (KJ1500604), the Chongqing Research Program of Basic Research and Frontier Technology (cstc2015jcyjA20013), the Program for Innovative Research Team in University in Chongqing (CXTDX201601003), and the 111 Project (B13041) is gratefully acknowledged.

References

[1] B. Weng, F. Xu, and J. Xu, "Hierarchical structures constructed by BiOX (X = Cl, I) nanosheets on CNTs/carbon composite fibers for improved photocatalytic degradation of methyl orange," *Journal of Nanoparticle Research*, vol. 16, no. 12, pp. 1–13, 2014.

[2] T. Xian, H. Yang, L. J. Di, and J. F. Dai, "Enhanced photocatalytic activity of BaTiO3@g-C3N4 for the degradation of methyl orange under simulated sunlight irradiation," *Journal of Alloys and Compounds*, vol. 622, pp. 1098–1104, 2015.

[3] A. Indra, P. W. Menezes, M. Schwarze, and M. Driess, "Visible light driven non-sacrificial water oxidation and dye degradation with silver phosphates: multi-faceted morphology matters," *New Journal of Chemistry*, vol. 38, no. 5, pp. 1942–1945, 2014.

[4] N. Song, H. Fan, and H. Tian, "PVP assisted in situ synthesis of functionalized graphene/ZnO (FGZnO) nanohybrids with enhanced gas-sensing property," *Journal of Materials Science*, vol. 50, no. 5, pp. 2229–2238, 2015.

[5] R. Chalasani and S. Vasudevan, "Cyclodextrin-functionalized Fe_3O_4@TiO_2: reusable, magnetic nanoparticles for photocatalytic degradation of endocrine-disrupting chemicals in water supplies," *ACS Nano*, vol. 7, no. 5, pp. 4093–4104, 2013.

[6] B. Liu, Z. Li, S. Xu, X. Ren, D. Han, and D. Lu, "Facile in situ hydrothermal synthesis of $BiVO_4$/MWCNT nanocomposites as high performance visible-light driven photocatalysts," *Journal of Physics and Chemistry of Solids*, vol. 75, no. 8, pp. 977–983, 2014.

[7] F. Dong, P. Li, J. Zhong et al., "Simultaneous Pd^{2+} doping and Pd metal deposition on $(BiO)_2CO_3$ microspheres for enhanced and stable visible light photocatalysis," *Applied Catalysis A: General*, vol. 510, pp. 161–170, 2016.

[8] Y. Sun, B. Qu, Q. Liu et al., "Highly efficient visible-light-driven photocatalytic activities in synthetic ordered monoclinic $BiVO_4$ quantum tubes–graphene nanocomposites," *Nanoscale*, vol. 4, no. 12, pp. 3761–3767, 2012.

[9] B. Zhang, Y. L. Wang, L. H. Huang, and S. Z. Tan, "Preparation and structure of $BiVO_4$-graphene composites," *Advanced Materials Research*, vol. 905, pp. 101–104, 2014.

[10] Q. Yu, Z.-R. Tang, and Y.-J. Xu, "Synthesis of BiVO4 nanosheets-graphene composites toward improved visible light photoactivity," *Journal of Energy Chemistry*, vol. 23, no. 5, pp. 564–574, 2014.

[11] X. J. Wang, H. L. Liu, X. L. Wan, J. R. Wang, and L. L. Chang, "Additive-free solvothermal synthesis of peanut-like BiVO4 powders with enhanced photocatalysis activity," *Crystal Research and Technology*, vol. 48, no. 12, pp. 1066–1072, 2013.

[12] M. Du, S. Xiong, T. Wu et al., "Preparation of a microspherical silver-reduced graphene oxide-bismuth vanadate composite and evaluation of its photocatalytic activity," *Materials*, vol. 9, no. 3, article 160, 2016.

[13] N. Bao, Z. Yin, Q. Zhang, S. He, X. Hu, and X. Miao, "Synthesis of flower-like monoclinic BiVO4/surface rough TiO2 ceramic fiber with heterostructures and its photocatalytic property," *Ceramics International*, vol. 42, no. 1, pp. 1791–1800, 2016.

[14] S. Dong, Y. Cui, Y. Wang et al., "Designing three-dimensional acicular sheaf shaped BiVO4/reduced graphene oxide composites for efficient sunlight-driven photocatalytic degradation of dye wastewater," *Chemical Engineering Journal*, vol. 249, pp. 102–110, 2014.

[15] X. Zhou, J. Yu, Y. Zhang, D. Yu, and W. Lu, "Enhancement in the photo-to-current efficiency by fabrication of CNT-$BiVO_4$ composites," *Rare Metals*, vol. 30, no. 1, pp. 199–202, 2011.

[16] Y. H. Ng, A. Iwase, A. Kudo, and R. Amal, "Reducing graphene oxide on a visible-light BiVO4 photocatalyst for an enhanced photoelectrochemical water splitting," *Journal of Physical Chemistry Letters*, vol. 1, no. 17, pp. 2607–2612, 2010.

[17] Y. Yan, S. Sun, Y. Song et al., "Microwave-assisted in situ synthesis of reduced graphene oxide-BiVO4 composite photocatalysts and their enhanced photocatalytic performance for the degradation of ciprofloxacin," *Journal of Hazardous Materials*, vol. 250-251, pp. 106–114, 2013.

[18] Y. Fu, X. Sun, and X. Wanga, "BiVO4-graphene catalyst and its high photocatalytic performance under visible light irradiation," *Materials Chemistry and Physics*, vol. 131, no. 1-2, pp. 325–330, 2011.

[19] P. Gao and D. D. Sun, "Hierarchical sulfonated graphene oxide-TiO_2 composites for highly efficient hydrogen production with a wide pH range," *Applied Catalysis B: Environmental*, vol. 147, pp. 888–896, 2014.

[20] M. S. Arif Sher Shah, K. Zhang, A. R. Park et al., "Single-step solvothermal synthesis of mesoporous Ag-TiO_2-reduced graphene oxide ternary composites with enhanced photocatalytic activity," *Nanoscale*, vol. 5, no. 11, pp. 5093–5101, 2013.

[21] H. Wang, L.-F. Cui, Y. Yang et al., "Mn_3O_4–graphene hybrid as a high-capacity anode material for lithium ion batteries," *Journal of the American Chemical Society*, vol. 132, no. 40, pp. 13978–13980, 2010.

[22] X. Xu, Q. Zou, Y. Yuan, F. Ji, Z. Fan, and B. Zhou, "Preparation of BiVO4-graphene nanocomposites and their photocatalytic activity," *Journal of Nanomaterials*, vol. 2014, Article ID 401697, 6 pages, 2014.

[23] X. Liu, L. Pan, T. Lv, Z. Sun, and C. Q. Sun, "Visible light photocatalytic degradation of dyes by bismuth oxide-reduced graphene oxide composites prepared via microwave-assisted method," *Journal of Colloid and Interface Science*, vol. 408, no. 1, pp. 145–150, 2013.

[24] P. Wang, J. Y. Zheng, D. Zhang, and Y. S. Kang, "Selective construction of junctions on different facets of $BiVO_4$ for enhancing photo-activity," *New Journal of Chemistry*, vol. 39, pp. 9918–9925, 2015.

[25] A. Zhang and J. Zhang, "Effects of europium doping on the photocatalytic behavior of $BiVO_4$," *Journal of Hazardous Materials*, vol. 173, no. 1–3, pp. 265–272, 2010.

[26] N. R. Khalid, E. Ahmed, Z. Hong, and M. Ahmad, "Synthesis and photocatalytic properties of visible light responsive La/TiO2-graphene composites," *Applied Surface Science*, vol. 263, pp. 254–259, 2012.

[27] M. Zalfani, B. Van Der Schueren, Z.-Y. Hu et al., "Novel 3DOM BiVO4/TiO2 nanocomposites for highly enhanced photocatalytic activity," *Journal of Materials Chemistry A*, vol. 3, no. 42, pp. 21244–21256, 2015.

[28] G. Zhu, Y. Liu, M. Hojamberdiev et al., "Thermodecomposition synthesis of porous β-Bi_2O_3/$Bi_2O_2CO_3$ heterostructured photocatalysts with improved visible light photocatalytic activity," *New Journal of Chemistry*, vol. 39, no. 12, pp. 9557–9568, 2015.

[29] W. Su, X. Lu, S. Jia, J. Wang, H. Ma, and Y. Xing, "Catalytic reduction of NOX over TiO_2–graphene oxide supported with MnOX at low temperature," *Catalysis Letters*, vol. 145, no. 7, pp. 1446–1456, 2015.

[30] Y. Xu, Y. Mo, J. Tian, P. Wang, H. Yu, and J. Yu, "The synergistic effect of graphitic N and pyrrolic N for the enhanced photocatalytic performance of nitrogen-doped graphene/TiO2 nanocomposites," *Applied Catalysis B: Environmental*, vol. 181, pp. 810–817, 2016.

[31] S. Yousefzadeh, M. Faraji, and A. Z. Moshfegh, "Constructing $BiVO_4$/Graphene/TiO_2 nanocomposite photoanode for photoelectrochemical conversion applications," *Journal of Electroanalytical Chemistry*, vol. 763, pp. 1–9, 2016.

[32] J. Han, G. Zhu, M. Hojamberdiev et al., "Rapid adsorption and photocatalytic activity for Rhodamine B and Cr(VI) by ultrathin BiOI nanosheets with highly exposed 001 facets," *New Journal of Chemistry*, vol. 39, no. 3, pp. 1874–1882, 2015.

[33] C. Yu, S. Dong, J. Zhao, X. Han, J. Wang, and J. Sun, "Preparation and characterization of sphere-shaped BiVO4/reduced graphene oxide photocatalyst for an augmented natural sunlight photocatalytic activity," *Journal of Alloys and Compounds*, vol. 677, pp. 219–227, 2016.

[34] Q. Shi, W. Zhao, L. Xie, J. Chen, M. Zhang, and Y. Li, "Enhanced visible-light driven photocatalytic mineralization of indoor toluene via a BiVO4/reduced graphene oxide/Bi2O3 all-solid-state Z-scheme system," *Journal of Alloys and Compounds*, vol. 662, pp. 108–117, 2016.

[35] K. Li, B. Chai, T. Peng, J. Mao, and L. Zan, "Preparation of $AgIn_5S_8$/TiO_2 heterojunction nanocomposite and its enhanced photocatalytic H_2 production property under visible light," *ACS Catalysis*, vol. 3, no. 2, pp. 170–177, 2013.

[36] O. F. Lopes, K. T. G. Carvalho, G. K. Macedo, V. R. De Mendonça, W. Avansi, and C. Ribeiro, "Synthesis of BiVO4 via oxidant peroxo-method: insights into the photocatalytic performance and degradation mechanism of pollutants," *New Journal of Chemistry*, vol. 39, no. 8, pp. 6231–6237, 2015.

[37] P. Luan, M. Xie, X. Fu, Y. Qu, X. Sun, and L. Jing, "Improved photoactivity of TiO_2-Fe_2O_3 nanocomposites for visible-light water splitting after phosphate bridging and its mechanism," *Physical Chemistry Chemical Physics*, vol. 17, no. 7, pp. 5043–5050, 2015.

[38] Y. Li, Y. Zhang, W. Ye, J. Yu, C. Lu, and L. Xia, "Photo-to-current response of $Bi_2Fe_4O_9$ nanocrystals synthesized through a chemical co-precipitation process," *New Journal of Chemistry*, vol. 36, no. 6, pp. 1297–1300, 2012.

[39] Z.-R. Tang, Q. Yu, and Y.-J. Xu, "Toward improving the photocatalytic activity of BiVO4-graphene 2D-2D composites under visible light by the addition of mediator," *RSC Advances*, vol. 4, no. 102, pp. 58448–58452, 2014.